

Optimal Fidelity Selection for Improved Performance in Human-in-the-Loop Queues for Underwater Search

Piyush Gupta

Vaibhav Srivastava

Abstract—In the context of human-supervised autonomy, we study the problem of optimal fidelity selection for a human operator performing an underwater visual search task. Human performance depends on various cognitive factors such as workload and fatigue. We perform human experiments in which participants perform two tasks simultaneously: a primary task, which is subject to evaluation, and a secondary task to estimate their workload. The primary task requires participants to search for underwater mines in videos, while the secondary task involves a simple visual test where they respond when a green light displayed on the side of their screens turns red. Videos arrive as a Poisson process and are stacked in a queue to be serviced by the human operator. The operator can choose to watch the video with either normal or high fidelity, with normal fidelity videos playing at three times the speed of high fidelity ones. Participants receive rewards for their accuracy in mine detection for each primary task and penalties based on the number of videos waiting in the queue. We consider the workload of the operator as a hidden state and model the workload dynamics as an Input-Output Hidden Markov Model (IOHMM). We use a Partially Observable Markov Decision Process (POMDP) to learn an optimal fidelity selection policy, where the objective is to maximize total rewards. Our results demonstrate improved performance when videos are serviced based on the optimal fidelity policy compared to a baseline where humans choose the fidelity level themselves.

Index Terms—workload, fidelity selection, Input-Output Hidden Markov Model (IOHMM), Partially Observable Markov Decision Process (POMDP)

I. INTRODUCTION

Human-in-the-loop systems have a wide range of applications, spanning from search and rescue missions [1] and airport security screening [2] to supervising robotic decision-making [3] and tele-driving of robot taxis [4]. In these systems, human operators frequently confront the challenge of processing substantial volumes of data, which can often lead to high workload conditions. Several factors, including visual limitations, attention bottlenecks, and fatigue, can contribute to performance deterioration, increasing the likelihood of errors. For instance, in an underwater search operation, a human operator may be required to review an extensive sequence of images or videos, resulting in a high workload and fatigue. Such conditions can lead to the unfortunate consequence of

missing the object of interest or an increased number of false alarms. Consequently, it becomes imperative to effectively manage the workload of the human operator to ensure the efficient execution of tasks with minimal errors.

We study the optimal fidelity selection for a human operator performing a visual search task, where fidelity refers to the level of precision and accuracy required for task completion. Specifically, we consider the task of underwater mine detection within videos produced from an underwater simulation. Videos arrive as a Poisson process and are stacked in a queue to be serviced by the human operator. The operator can select either normal or high fidelity to view the videos. Notably, normal-fidelity videos are played at three times the speed of high-fidelity ones. This setting presents a trade-off, where high-fidelity viewing can potentially enhance task accuracy at the cost of increasing the queue size and slowing down task processing. We elucidate this trade-off by studying the policy for optimal fidelity selection.

In addition to fidelity levels, the performance of the task can be significantly affected by the workload of the human operator. For instance, a human operator under high workload conditions is more likely to commit errors when executing the task with normal fidelity, compared to when they are in a normal workload state. Therefore, it becomes essential to develop an optimal fidelity selection policy that takes into account both the number of pending tasks (queue length) and the workload of the human operator to improve the system's performance.

There are a variety of methods used for estimating the human workload. Physiological sensors like electroencephalography (EEG) [5], [6], electrocardiogram (ECG) [7], [8], galvanic skin response (GSR) [9], and eye trackers [10], [11] are frequently employed to assess the operator's cognitive condition. Many features such as power spectral density from EEG, heart rate, respiration rate, galvanic skin response, blink rates, pupil diameter, etc. are utilized to identify physiological and cognitive precursors to behavior, such as fatigue, or situational awareness [12], [13], [14]. However, it's worth noting that these measures rely on costly hardware, which can limit their applicability in various real-world scenarios, particularly when a human operator is supervising remotely. Consequently, instead of gauging workload through expensive sensors, an alternative approach involves estimating it by observing the reaction time of the human operator while performing a secondary task.

Recent years have seen significant efforts in effectively

This work has been supported in part by the NSF awards IIS-1734272 and ECCS-2024649. The analysis portion of this work is supported in part by the ONR award N00014-22-1-2813.

Piyush Gupta (guptapi1@msu.edu) and Vaibhav Srivastava (vaibhav@egr.msu.edu) are with Department of Electrical and Computer Engineering, Michigan State University, East Lansing, Michigan, 48824, USA.

managing human cognitive resources to optimize the system performance [2], [15]. The problem of optimal fidelity selection has been studied in [16], where the authors establish the structural properties of the optimal policy. However, the authors assume a known cognitive dynamics of the human operator which is modeled as a Markov chain. Other studies in this domain include optimal scheduling of the tasks to be serviced by the operator [17], enabling shorter operator reaction times by controlling the task release [18], and determining optimal operator attention allocation [19]. In contrast to these works, we assume the human workload as a hidden state and focus on the human experiments. Specifically, we study the impact of optimal fidelity selection policy on human performance in the experiments.

In this work, we consider the workload of the human operator as a hidden state. We employ an Input-Output Hidden Markov Model (IOHMM) [20], [21], [22] to capture the operator’s workload dynamics, where the hidden workload is influenced by input fidelity levels. This hidden state impacts the operator’s performance in primary and secondary tasks, which we use as observations to estimate the hidden workload. Using the state and observation dynamics learned from IOHMM, we utilize a Partially Observable Markov Decision Process (POMDP) [23], [24], [25] to obtain an optimal fidelity selection policy. Our experimental findings demonstrate a substantial enhancement in human performance when utilizing an optimal policy, in contrast to relying on a policy chosen by the individuals themselves.

This work presents three major contributions. First, we address the optimal fidelity selection challenge by framing it as a control of a queue problem, with a hidden server workload state. We employ IOHMM and POMDP to derive the optimal fidelity selection policy. Second, we compare the human fidelity selection policy with the optimal policy and draw valuable insights into human behavioral patterns. Third, we illustrate that by recommending the optimal policy, a decision support system can effectively aid human decision-making, leading to a substantial improvement in their performance.

The rest of the manuscript is structured as follows. In Section II, we introduce our problem setup and present some mathematical preliminaries. Section III outlines the design of our human experiments and provides information about our experimental setup. Section IV delves into our primary findings, including a comparative analysis of system performance under both human and optimal policies. Finally, we conclude in Section V.

II. BACKGROUND AND PROBLEM FORMULATION

We now discuss our problem setup, formulate it as POMDP, and solve it to obtain the optimal fidelity selection policy.

A. Problem Setup

We study the problem of optimal fidelity selection for a human operator performing a visual search task. The human operator performs two tasks simultaneously, a primary task and a secondary task. The primary task involves searching for underwater mines in videos generated from an underwater

simulation designed using Gazebo [26] and ROS [27]. The operator watches videos and responds by pressing a key whenever a mine is spotted. On the other hand, the secondary task involves a simple visual exercise, where participants press a key as early as possible when a green light located at the side of the screen changes to red. During each primary task, the green light undergoes this transition randomly, occurring between the 25% and 75% mark of the video. We record the participants’ reaction time in the secondary tasks, and in a rare event when a participant misses the red light, the reaction time is set to the total time the light stays red until the end of the primary task.

Fig. 1 shows the experiment interface. The videos for the primary task arrive as a Poisson process with an arrival rate of $\lambda \in \mathbb{R}_{>0}$ and get stacked in a queue awaiting service by the human operator. The operator has the option to select either high or normal fidelity levels for servicing each video. In normal fidelity, the video is presented at a speed of three times faster compared to high-fidelity processing. Additionally, operators can choose to delegate a task for autonomous processing, even though the accuracy of the autonomous system may be lower. This delegation or “skip” action serves as a means to maintain queue stability, especially in situations with large queue lengths.

The performance of a human operator relies on their workload, making it a crucial factor in our problem formulation. To address this, we formulate the problem as a POMDP, with the workload of the operator treated as a latent or hidden variable. We estimate this hidden workload through a combination of reaction time measurements from the secondary task and performance metrics obtained from the primary task. Specifically, we model the workload dynamics of the human operator using an IOHMM (see Fig. 2). In this model, the fidelity level a serves as the input, the workload w operates as the hidden state, and we observe three distinct output measures o^1, o^2, o^3 . These output measures correspond to the fraction of correctly detected mines in the primary task, the count of false alarms in the primary task, and the reaction time recorded during the execution of the secondary task, respectively. This modeling approach helps us understand how fidelity, workload, and task performance are interconnected in one unified framework.

We utilize the extended Baum-Welch algorithm [21] to train the IOHMM model, which provides the transition probabilities $p(w'|w, a)$, observation probabilities $p(o|w, a)$, and the initial state distribution $p(w_0)$ through expectation maximization. These probabilities are utilized in the POMDP formulation to obtain the optimal fidelity selection policy.

To determine the most suitable number of hidden workload states, we use the Akaike information criterion (AIC) [28] and Bayesian information criterion (BIC) [29] for model selection. For a given number of hidden states, the AIC and BIC are defined as:

$$AIC = 2p - 2\log(\hat{\mathcal{L}}), \quad BIC = p\log(n_o) - 2\log(\hat{\mathcal{L}}), \quad (1)$$

where p represents the number of learned parameters, n_o stands for the number of observation trajectories, and $\hat{\mathcal{L}}$ signifies the maximized value of the log-likelihood function derived from the trained model. The model with the lowest AIC (or

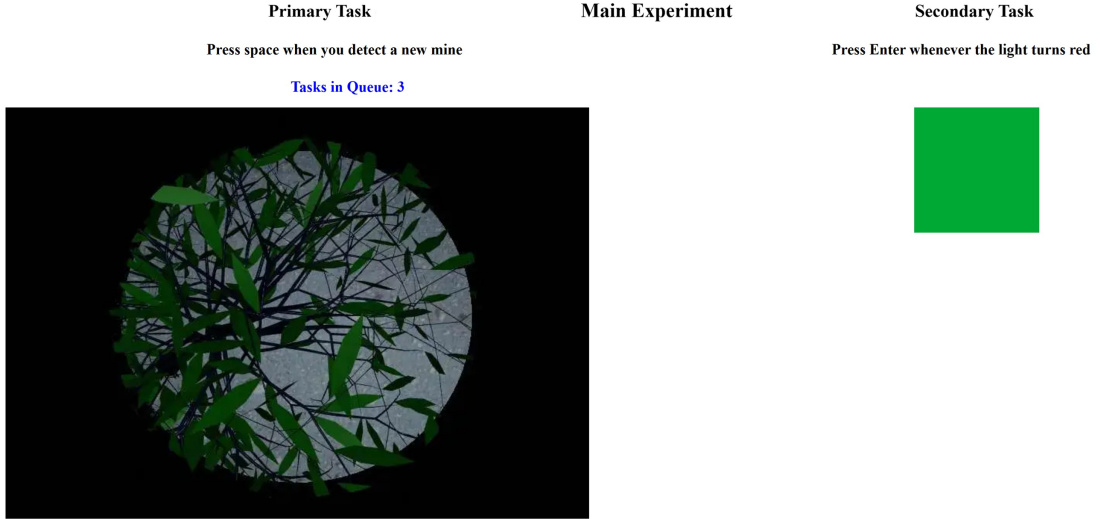


Fig. 1: Human experiment interface. The participants press the spacebar key whenever a new mine is detected in the primary task video. Additionally, the green light (secondary task) randomly turns red once for each primary task and the participant responds by pressing the Enter key as early as possible. The queue length (tasks waiting in the queue) is displayed on top of the primary task.

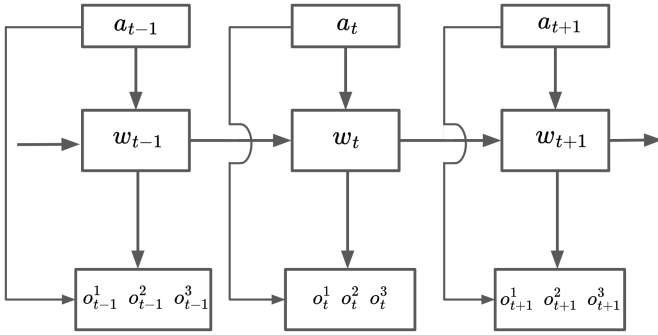


Fig. 2: Input-output hidden Markov model. The input a represents the fidelity level, the hidden state w signifies the workload, and the three observations o^1 , o^2 , and o^3 correspond to the fraction of correctly detected mines in the primary task, the count of false alarms in the primary task, and the reaction time recorded during the execution of the secondary task, respectively.

BIC) value is considered the optimal choice, as determined by the AIC (or BIC) criteria. Based on these criteria (presented in Section III-C), we train an IOHMM model with two hidden states, which we refer to as normal and high workload states.

B. Mathematical Modeling

We formulate our problem as a POMDP $\mathcal{P} = \{\mathcal{S}, \mathcal{A}, \Omega, \mathcal{T}, \mathcal{O}, r, \gamma\}$, where \mathcal{S} is the state space, \mathcal{A} in the action space, Ω is the set of observations, \mathcal{T} is the set of conditional transition probabilities between states, \mathcal{O} is the set of conditional observation probabilities, $r : \mathcal{S} \times \mathcal{A} \rightarrow \mathbb{R}$ is the reward function, and $\gamma \in [0, 1)$ is the discount factor. The state space of the system is defined using a tuple $\mathcal{S} = (q, w)$, where $q \in \{0, 1, \dots, L\}$ and $w \in \mathcal{W} = \{0, 1\}$ denotes the number of tasks waiting in the queue (with maximum queue length L) and the hidden discrete workload of the human operator, respectively. We define $w = 0$ as the normal workload state and $w = 1$ as the high workload state. The action space is defined as $\mathcal{A} = \{N, H, D\}$, with N and H representing

normal and high-fidelity task processing, respectively. The action D corresponds to task delegation, allowing the task to be handled by autonomous systems. This delegation action is particularly useful for maintaining queue stability when dealing with a large queue length. To discourage excessive use of the delegation action, we assume that the autonomy's accuracy in mine detection is significantly lower which results in a lower immediate reward.

The observation space is defined by a tuple $\Omega = (o^1, o^2, o^3)$, where o^1 , o^2 , and o^3 correspond to the fraction of correctly detected mines in the primary task, the count of false alarms in the primary task, and the reaction time recorded during the execution of the secondary task, respectively. The state transition probability $p(s'|s, a) \in \mathcal{T}$ is derived from the queue dynamics $p(q'|q, a)$ given by the Poisson distribution with arrival rate λt , where t is the duration of the task, and workload dynamics $p(w'|w, a)$ obtained by training the IOHMM. The observation probabilities $p(o|s', a) = p(o^1, o^2, o^3|w', a) \in \mathcal{O}$ are also obtained from the trained IOHMM model. The observation probabilities are assumed to be independent of the queue length, and therefore, only depend on the workload of the operator, i.e., $p(o|s', a) = p(o|w', a)$. We define the reward function as $r(s, a) = \alpha_1 o^1 - \alpha_2 o^2 - \alpha_3 q$, where α_i for $i \in \{1, 2, 3\}$ are positive constants, which rewards high accuracy in the primary task and penalizes for the number of tasks waiting in the queue.

We convert the POMDP to a belief MDP defined by $\mathcal{M} = \{\mathcal{B}, \mathcal{A}, \tau, r, \gamma\}$. Here, $\mathcal{B} := \{(q, b_H) \mid q \in \{0, 1, \dots, L\}, b_H \in \Delta_D\}$ is the new state space, where q is the original queue length, b_H is the discrete belief probability for being in the high workload state, and Δ_D is a discretization of the interval $[0, 1]$. Therefore, the belief probability for being in the normal workload state is given by $1 - b_H$. For our experiments, we discretize $[0, 1]$ with a step size of 0.1, i.e., $\Delta_D = \{0, 0.1, \dots, 1\}$. Note that the discretization of b_H results in a finite state space \mathcal{B} . Let $b : \mathcal{W} \rightarrow \Delta_D$ denote

the belief vector, where $b(0) = 1 - b_H$, and $b(1) = b_H$. From a current belief $b(w)$, taking an action a and observing o , the updated belief $b'(w')$ is given by:

$$b'(w') = \eta p(o|w', a) \sum_{w \in \mathcal{W}} p(w'|w, a) b(w), \quad (2)$$

where $\eta = \frac{1}{p(o|b, a)}$ is the normalizing constant with

$$p(o|b, a) = \sum_{w' \in \mathcal{W}} p(o|w', a) \sum_{w \in \mathcal{W}} p(w'|w, a) b(w). \quad (3)$$

The updated belief probabilities in $b'(w')$, where $b'(0) = 1 - b'_H$ and $b'(1) = b'_H$ obtained from (2) are mapped to the closest discrete states such that $b'_H \in \Delta_D$. The action set \mathcal{A} is the original action space. The transition probabilities $\tau(q', b'|q, b, a) = p(q'|q, a) p(b'|b, a)$ is composed of the Poisson process for queue dynamics $p(q'|q, a)$, and the workload dynamics $p(b'|b, a)$, which is given by:

$$p(b'|b, a) = \sum_{o \in \mathcal{O}} p(b'|b, a, o) p(o|b, a), \quad (4)$$

where

$$p(b'|b, a, o) = \begin{cases} 1, & \text{if belief update in (2) returns } b', \\ 0, & \text{otherwise,} \end{cases} \quad (5)$$

and $p(o|b, a)$ is defined in (3). The reward function $r : \mathcal{B} \times \mathcal{A} \rightarrow \mathbb{R}$ is given by:

$$r(q, b_H, a) = \sum_{s \in \mathcal{S}|w=0} r(s, a) (1 - b_H) + \sum_{s \in \mathcal{S}|w=1} r(s, a) b_H, \quad (6)$$

where $r(s, a)$ is the original reward function for the POMDP. The discount factor γ is the original discount factor of the POMDP. For the belief MDP \mathcal{M} , the expected value for policy π starting from an initial state $(q_0, b_{H,0})$ is defined as:

$$\begin{aligned} V^\pi(q_0, b_{H,0}) &= \sum_{t=0}^{\infty} \gamma^t r(q_t, b_{H,t}, a_t) \\ &= \sum_{t=0}^{\infty} \gamma^t \mathbb{E}[r(s_t, a_t) | q_0, b_{H,0}, \pi], \end{aligned} \quad (7)$$

where the expectation is computed over $(q_t, b_{H,t}, w_t)$. The optimal fidelity selection policy maximizes the value in each belief state, i.e.,

$$\pi^* = \arg \max_{\pi} V^\pi(q_0, b_{H,0}).$$

We utilize the value iteration algorithm to solve the belief MDP and obtain the optimal fidelity selection policy.

III. HUMAN EXPERIMENTS

In this section, we discuss the design of our human experiments conducted using Prolific (www.prolific.com).

A. Experimental Setup

We developed an underwater mine search experiment within the Robot Operating System (ROS) framework using Gazebo models. For our simulation, we employed the ‘‘UUV simulator’’ [30], a comprehensive package encompassing Gazebo plugins and ROS nodes specifically tailored for simulating unmanned underwater vehicles, including remotely operated vehicles (ROVs) and autonomous underwater vehicles (AUVs).

In our experimental setup, we designed an underwater scenario where we placed underwater mines randomly throughout the environment following a uniform distribution within a predefined area. To increase the complexity of the task, we also randomly introduced a significant amount of underwater vegetation, which added an extra layer of difficulty in detecting the mines.

We captured underwater videos by deploying an ROV into the environment. The ROV followed a predetermined circular trajectory as it moved through the underwater space. Equipped with a downward-facing camera, the ROV recorded images. To ensure optimal recording conditions, we maintained complete darkness in the environment. The sole source of illumination was a single light attached to the ROV, directing its beam vertically downward. Consequently, only the area directly beneath the ROV was within the recording scope, resulting in a focused and well-illuminated view. We recorded a total of 5600 images which are used as 56 videos, with each video consisting of 100 frames. Fig. 3 shows example image frames containing underwater mines recorded from ROV. The mines’ positions are highlighted within red bounding boxes in the frames.

We performed 5 set of experiments, with each experiment group consisting of 20 participants. In each experiment, the participants first performed 8 practice tasks followed by 48 main tasks, where each task consists of a primary and a secondary task. Following is the list of experiments.

- *Experiment 1*: The first experiment was the base experiment where we recorded data to train the IOHMM model and learn the optimal fidelity selection policy by solving the POMDP. In this experiment, the 48 videos were evenly divided, with half of them being displayed at normal fidelity and the other half at high fidelity. To maintain consistency and balance, the tasks were presented in alternating blocks of four tasks each. Specifically, the sequence of 48 tasks was organized as $\{N, N, N, N, H, H, H, H, \dots\}$ for half of the participants and $\{H, H, H, H, N, N, N, N, \dots\}$ for another half of the participants. This reversal was thereby used to prevent ordering bias in our estimates.
- *Experiment 2*: In this experiment, the participants were allowed to choose a fidelity level for servicing each task. Before releasing each task, the participant decided on their desired fidelity level by pressing a key. This served as a baseline, where the human operator received no decision support. In this experiment, we do not allow task delegation, and the participants were only allowed to choose to service each task with either a normal or high fidelity level.

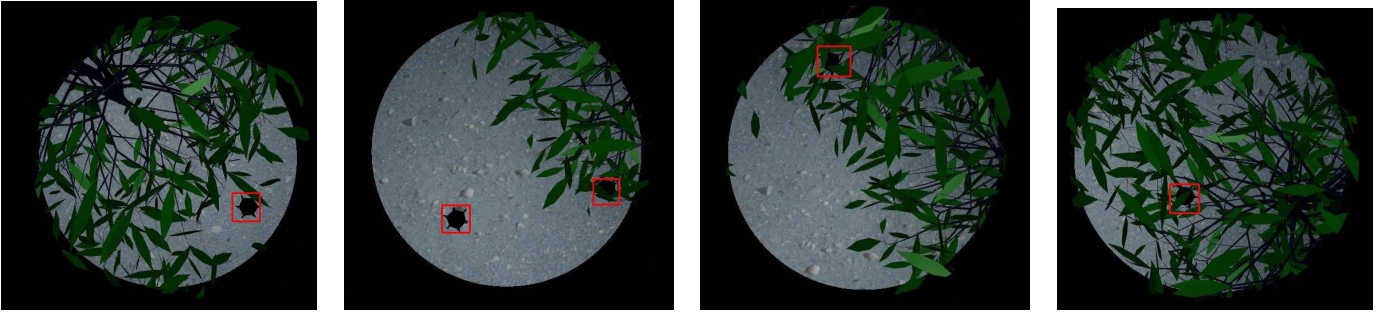


Fig. 3: Example image frames containing mines recorded from ROV. The mines' positions are highlighted within red bounding boxes in the frames.

- *Experiment 3*: In this experiment, the decision support system determined the appropriate fidelity level for each task by considering both the current operator performance and the queue length. Specifically, the decision support system monitored the operator's performance in each task, updated its belief using (2), and selected the optimal action in accordance with the optimal fidelity selection policy. For this experiment, we utilized an optimal policy that comprises only two available actions: normal and high fidelity.
- *Experiment 4*: This experiment was similar to Experiment 2, with the modification that the participants were provided an additional action of delegating the task to the autonomous system.
- *Experiment 5*: This experiment was similar to Experiment 3, with the modification that the optimal policy consisting of three actions: normal fidelity, high fidelity, and task delegation was used to choose the fidelity level for each task.

B. Methods

After receiving the IRB consent (MSU IRB #9452) from Michigan State University's IRB office, we recruited 100 participants using Prolific for the study. Inclusion criteria were established as having completed a minimum of 500 prior studies and maintaining a 99% approval rate on the platform. Participants were compensated with a base payment of \$6 and had the opportunity to earn additional performance-based bonuses ranging from \$0 – \$4.

C. IOHMM results

We use the data from Experiment 1 to train IOHMM models with different numbers of hidden states. Table I illustrates the AIC and BIC values (normalized with the number of observation trajectories) for the trained IOHMM models with 2, 3, and 4 hidden workload states, respectively. Based on the AIC and BIC criterion, we utilize a trained IOHMM model with two hidden states, which we refer to as normal and high workload states.

Fig. 4a and 4b show the workload transition diagram for the trained IOHMM model under normal and high fidelity, respectively. Under high fidelity, due to the slower speed of videos, there is a higher probability of transitioning from the

Hidden States	2	3	4
AIC	735.29	735.91	736.28
BIC	736.39	737.85	739.26

TABLE I: AIC and BIC values for model selection

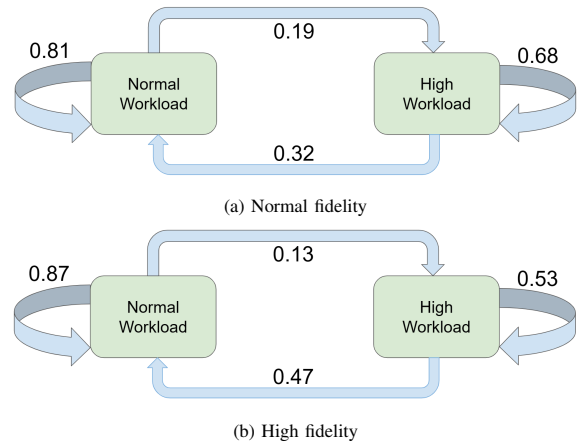


Fig. 4: Workload transition diagram under (a) normal and (b) high fidelity servicing of tasks.

high workload state to a lower workload state as compared to under normal fidelity. Similarly, the probability of transitioning into a high workload state from the normal workload state is higher under normal fidelity as compared to the high fidelity servicing. In the case of task delegation action, the task is instantaneously removed from the queue and hence, we assume that the workload remains the same under task delegation.

For observations o^1 , o^2 , and o^3 , we learn a normal distribution with unknown mean and standard deviation for each state-action pair. Fig. 5a and 5b present the reaction time distributions for normal and high fidelity, respectively. We identify state 0 as a normal workload state, while state 1 represents the high workload state. The mean and the variance of the reaction time in the secondary task are larger in the high workload state than in the normal workload state.

Fig. 6a and 6b depict the distributions for the fraction of detected mines in the primary task for normal and high fidelity, respectively. Notably, we observe a substantial difference in the means of the fraction of detected mines between normal and high workload states under normal fidelity. In contrast,

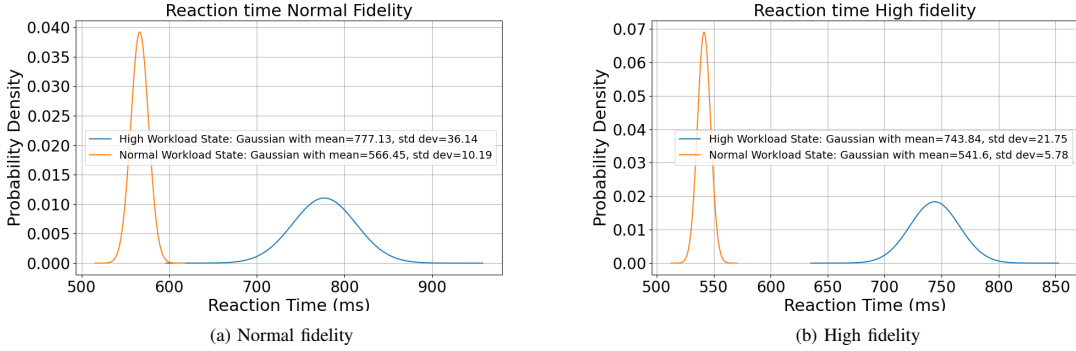


Fig. 5: Reaction time diagram under (a) normal and (b) high fidelity servicing of tasks.

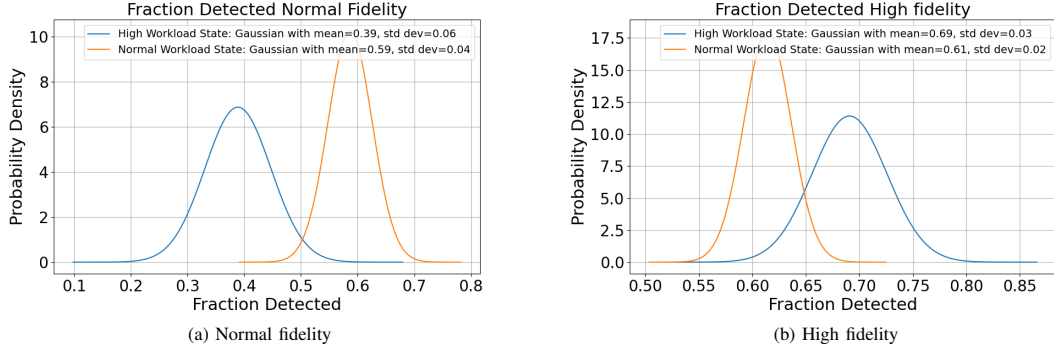


Fig. 6: Fraction of mines detected in primary task under (a) normal and (b) high fidelity servicing of tasks.

the means are relatively similar between these states under high fidelity. This observation suggests that when we do not take into account the penalty associated with the queue length, choosing high fidelity (slower videos) could be a suitable action during high workload conditions.

Fig. 7a and 7b illustrate the distributions for the number of false alarms in the primary task for normal and high fidelity, respectively. Notably, in the normal workload state, no false alarms were recorded. Therefore, in the normal workload state, we replace the normal distribution with a Dirac delta function that yields a probability of 1 at 0 false alarms and 0 everywhere else.

Finally, the initial distribution for the workload was determined as $[0.662, 0.338]$, where 0.662 is the probability of starting in a normal workload state. To solve the POMDP, we discretize the distributions of the reaction time, fraction of mines detected, and the false alarms, with a step size of 25 ms, 0.05, and 0.5, respectively.

D. Optimal Policy

Using the distributions from trained IOHMM, we convert the POMDP into a belief MDP as detailed in Sec. II-B. We utilize the following reward function:

$$r(s, a) = \begin{cases} 100o^1 - 30o^2 - 2q, & \text{for } a \in \{N, H\}, \\ 30 - 2(q - 1), & \text{for } a = D, \end{cases} \quad (8)$$

where we assumed the accuracy of autonomous servicing (task delegation) to be just 30%. We employed the value iteration algorithm to derive an optimal fidelity selection policy.

We developed two optimal policies: one with only two available actions and another with three available actions, including task delegation.

Fig. 8a and 8b illustrate the optimal policy with two and three available actions, respectively. In situations characterized by low queue lengths and a higher level of belief that workload is high, opting for high-fidelity servicing emerges as the optimal action. For other regions of the state space, normal fidelity servicing is the optimal action. When task delegation is a viable option, it becomes the optimal action only when there is a near certainty of being in the high workload state, as indicated by a belief close to 1, and the queue length is substantial.

IV. RESULTS

We now discuss the results of the experiments.

Fig. 9 compares the policy utilized in Experiments 2 and 3 that only allowed servicing a task with either normal or high fidelity. Fig. 9a, 9b, and 9c show the empirical human policy obtained from Experiment 2 data, complete optimal policy learned from POMDP, and the empirical policy obtained using data from Experiment 3 that deploys optimal fidelity selection policy, respectively. The two columns of the plots show the probability of choosing high-fidelity action and normal-fidelity action, respectively. The dark purple region in

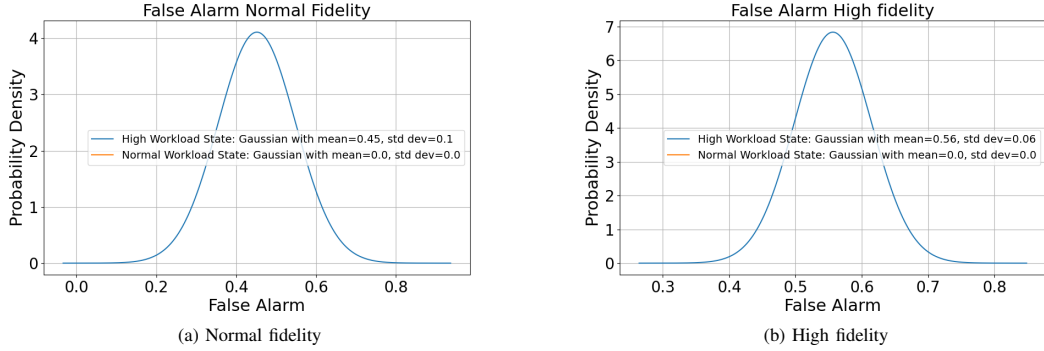


Fig. 7: Number of false alarms in primary task under (a) normal and (b) high fidelity servicing of tasks.

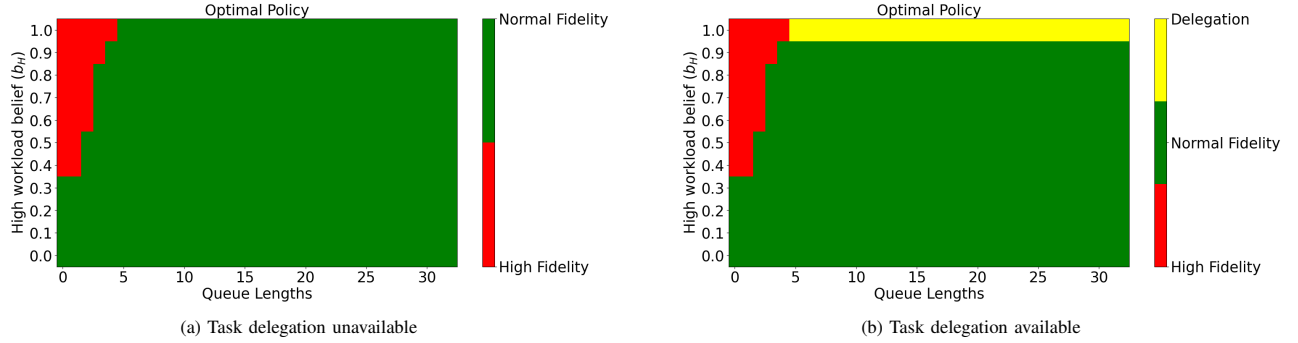


Fig. 8: Optimal fidelity selection policy where the action space (a) does not include task delegation and (b) includes task delegation

the plots represents the portions of the state space that have not been visited during the experiment.

By comparing the human policy with the optimal policy, we can gain important insights into human behavioral patterns. It is evident that the human policy exhibits minimal variation in fidelity with respect to the queue length. This suggests that humans struggle to effectively balance the trade-off between their ongoing tasks and the pending tasks in the queue.

Furthermore, human policy reveals a tendency for high-fidelity servicing in low-workload states and normal-fidelity servicing in high-workload states. This implies that humans tend to have difficulty switching between actions. Participants who prioritize high accuracy in primary tasks opt for high-fidelity servicing, resulting in normal workload conditions. Conversely, those who prioritize speed choose normal fidelity servicing, which can lead to operating under high workload conditions. Consequently, humans appear to have difficulty accurately assessing their workload and performance, hampering their ability to switch actions effectively.

Lastly, the empirical policy obtained using data from Experiment 3 indicates that the optimal policy effectively manages the queue length, thereby keeping the region of high queue length unexplored during the experiment.

Fig. 10 presents the comparative box plots for the scores obtained in Experiment 2 (human policy) and Experiment 3 (optimal policy). Here, the score refers to the cumulative reward accrued by a participant over tasks, i.e., $\text{Score} = \sum_{t=1}^{48} r_t$, where r_t denotes the reward obtained for servicing the task t given by (8). It can be seen that the performance

under optimal policy is much better than the performance under human policy. Furthermore, under the optimal policy, we observe an improvement of 26.54% in the average total score as compared to the human policy.

To assess the statistical significance of these findings, we conducted a two-sample t -test comparing the outcomes of Experiments 2 and 3. Remarkably, the p value was computed as 0.017, indicating a notably high level of significance. In line with the widely accepted significance threshold of 0.05, a p value below this threshold prompts us to reject the null hypothesis. This implies that the data from the two experiments do not stem from the same distribution at a 5% significance level. These results underscore the substantial impact of the optimal policy in enhancing human performance.

Next, we allow an additional action of task delegation under which a task is instantaneously removed from the queue to be serviced by the autonomy. Fig. 11 compares the policy utilized in Experiments 4 and 5 that allowed all three actions. Fig. 11a, 11b, and 11c show the empirical human policy obtained using data from Experiment 4, complete optimal policy learned from POMDP, and the empirical policy obtained using data from Experiment 3 that deploys optimal fidelity selection policy, respectively. The three columns of the plots show the probability of choosing high-fidelity action, normal-fidelity action, and task delegation, respectively. The dark purple region in the plots represents the portions of the state space that have not been visited during the experiment.

Similar observations to those depicted in Fig. 9 can also be made for high and normal fidelity servicing in Fig. 11.

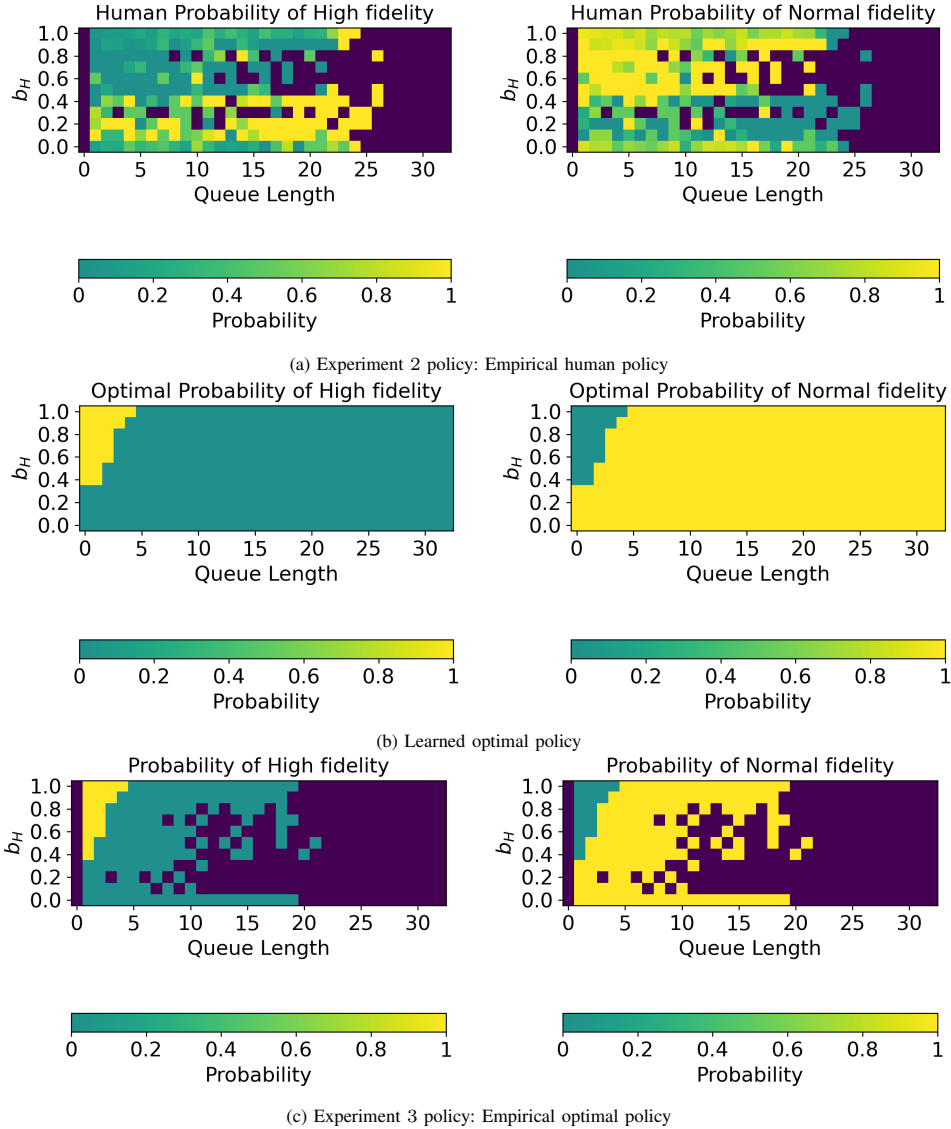


Fig. 9: (a) Empirical human policy in Experiment 2, (b) Learned optimal policy by solving POMDP with two available actions, and (c) Empirical policy obtained using data from Experiment 3 that deploys optimal fidelity selection policy.

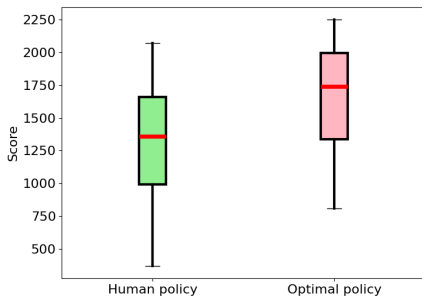


Fig. 10: Box plots for the participants' scores in Experiment 2 (human policy) and Experiment 3 (optimal policy). Within each box plot, the median is represented by the red horizontal line, while the lower and upper edges of the box signify the 25th and 75th percentiles, respectively. Whiskers extend to encompass the most extreme data points. The p value in the two-sample t -test comparing the outcomes of Experiments 2 and 3 was computed as 0.017, indicating a high level of statistical significance.

Moreover, it is noticeable that the human policy exhibits a somewhat random utilization of task delegation. This observation suggests that humans struggle with workload management and effective task delegation. Lastly, the optimal policy in Experiment 5 keeps the queue length under check, and therefore, regions of higher queue lengths remain unvisited in the experiment.

Fig. 12 shows the box plots for the participants' scores in Experiment 4 (human policy) and Experiment 5 (optimal policy). It can be seen that the performance under optimal policy is much better than the performance under human policy. Furthermore, under the optimal policy, we observe an improvement of 50.3% in the average total score as compared to the human policy. Lastly, the p -value in the two-sample t -test is given by 0.001, showing that the results are statistically significant.

Remark 1. *The average score achieved with the optimal policy in Experiment 5 was marginally less than that obtained*

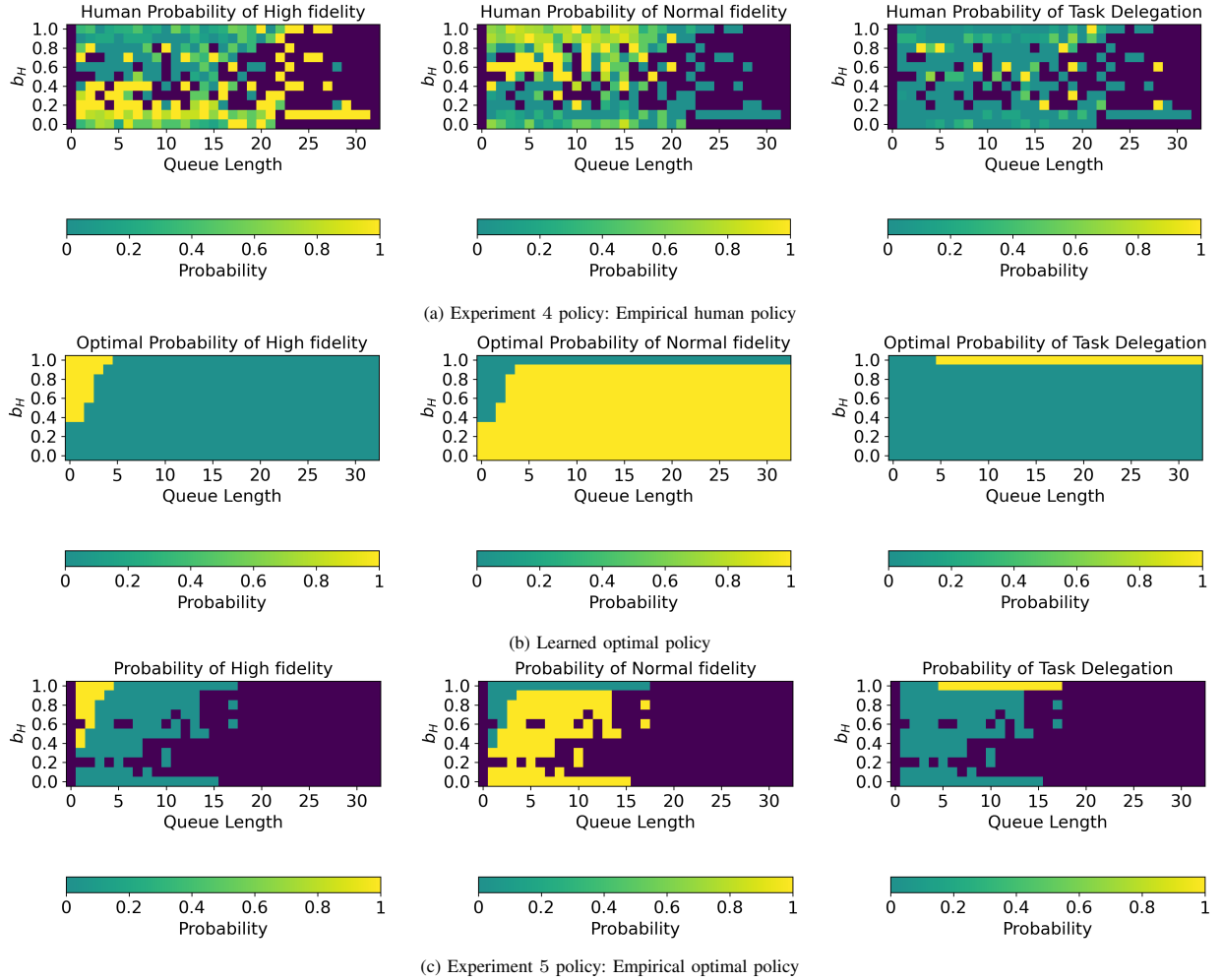


Fig. 11: (a) Empirical human policy in Experiment 4, (b) Learned optimal policy by solving POMDP with three available actions, and (c) Empirical policy obtained using data from Experiment 5 that deploys optimal fidelity selection policy.

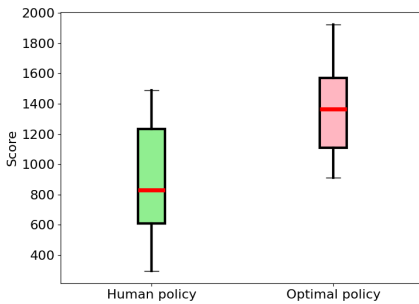


Fig. 12: Box plots for the participants' scores in Experiment 4 (human policy) and Experiment 5 (optimal policy). Within each box plot, the median is represented by the red horizontal line, while the lower and upper edges of the box signify the 25th and 75th percentiles, respectively. Whiskers extend to encompass the most extreme data points. The p value in the two-sample t-test comparing the outcomes of Experiments 4 and 5 was computed as 0.001, indicating a high level of statistical significance.

with the optimal policy in Experiment 3. This discrepancy could be due to the relatively smaller reward obtained from task delegation, as opposed to servicing the task with normal fidelity. Although the optimal policy in Experiment 5 may

default to task delegation under the presumption of diminished performance during periods of high workload, certain participants may demonstrate the capability to execute tasks with high accuracy even under high workload conditions in Experiment 3.

V. CONCLUSIONS

We studied the problem of optimal fidelity selection for a human operator engaged in a visual search task. The human participants performed two tasks simultaneously: a primary mine search task, and a secondary visual task used for estimating the human workload. We treated the human workload as a hidden state and modeled the workload dynamics using an Input-Output Hidden Markov Model (IOHMM). Leveraging the probability distributions derived from the IOHMM, we formulated a Partially Observable Markov Decision Process (POMDP) and solved it to derive an optimal fidelity selection policy. The results of our experiments offer valuable insights into human behavioral patterns and underscore the substantial performance enhancements achievable through the application of the optimal policy.

REFERENCES

- [1] Y. Nevatia, T. Stoyanov, R. Rathnam, M. Pfingsthorn, S. Markov, R. Ambrus, and A. Birk, "Augmented autonomy: Improving human-robot team performance in urban search and rescue," in *International Conference on Intelligent Robots and Systems*, pp. 2103–2108, IEEE, 2008.
- [2] P. Gupta and V. Srivastava, "Optimal fidelity selection for human-in-the-loop queues using semi-Markov decision processes," in *American Control Conference*, pp. 5266–5271, IEEE, 2019.
- [3] T. Kaupp, A. Makarenko, and H. Durrant-Whyte, "Human–robot communication for collaborative decision making—a probabilistic approach," *Robotics and Autonomous Systems*, vol. 58, no. 5, pp. 444–456, 2010.
- [4] O. Amador, M. Aramrattana, and A. Vinel, "A survey on remote operation of road vehicles," *IEEE Access*, vol. 10, pp. 130135–130154, 2022.
- [5] R. Singla, A. Agrawal, V. Kumar, and O. P. Verma, "Real-time mental workload detector for estimating human performance under workload," in *Advances in Signal Processing and Communication: Select Proceedings of ICSC*, pp. 383–392, Springer, 2019.
- [6] A.-M. Brouwer, M. A. Hogervorst, J. B. Van Erp, T. Heffelaar, P. H. Zimmerman, and R. Oostenveld, "Estimating workload using EEG spectral power and ERPs in the n-back task," *Journal of Neural Engineering*, vol. 9, no. 4, p. 045008, 2012.
- [7] A. Tjolleng, K. Jung, W. Hong, W. Lee, B. Lee, H. You, J. Son, and S. Park, "Classification of a driver's cognitive workload levels using artificial neural network on ECG signals," *Applied Ergonomics*, vol. 59, pp. 326–332, 2017.
- [8] H. Qu, X. Gao, and L. Pang, "Classification of mental workload based on multiple features of ECG signals," *Informatics in Medicine Unlocked*, vol. 24, p. 100575, 2021.
- [9] J. Zhou, J. Y. Jung, and F. Chen, "Dynamic workload adjustments in human-machine systems based on GSR features," in *Human-Computer Interaction-INTERACT*, pp. 550–558, Springer, 2015.
- [10] A. Pradhan and E. Kumar, "Cognitive workload estimation using eye tracking: A review," in *International Conference on Advancements in Interdisciplinary Research*, pp. 544–552, Springer, 2022.
- [11] R. Luo, Y. Weng, P. Jayakumar, M. J. Brudnak, V. Paul, V. R. Desaraju, J. L. Stein, T. Ersal, and X. J. Yang, "Real-time workload estimation using eye tracking: A Bayesian inference approach," *International Journal of Human-Computer Interaction*, pp. 1–16, 2023.
- [12] J. Heard, C. E. Harriott, and J. A. Adams, "A survey of workload assessment algorithms," *IEEE Transactions on Human-Machine Systems*, vol. 48, no. 5, pp. 434–451, 2018.
- [13] T. Kosch, J. Karolus, J. Zagermann, H. Reiterer, A. Schmidt, and P. W. Woźniak, "A survey on measuring cognitive workload in human-computer interaction," *ACM Computing Surveys*, 2023.
- [14] V. J. Gawron, *Workload Measures*. CRC Press, 2019.
- [15] P. Gupta and V. Srivastava, "On robust and adaptive fidelity selection for human-in-the-loop queues," in *European Control Conference*, pp. 872–877, 2021.
- [16] P. Gupta and V. Srivastava, "Structural properties of optimal fidelity selection policies for human-in-the-loop queues," *Automatica*, vol. 159, p. 111388, 2024. Extended version available at: arXiv preprint arXiv: 2201.09990.
- [17] J. R. Peters, A. Surana, and F. Bullo, "Robust scheduling and routing for collaborative human/unmanned aerial vehicle surveillance missions," *Journal of Aerospace Information Systems*, pp. 1–19, 2018.
- [18] K. Savla and E. Frazzoli, "A dynamical queue approach to intelligent task management for human operators," *Proceedings of the IEEE*, vol. 100, no. 3, pp. 672–686, 2012.
- [19] V. Srivastava, R. Carli, C. Langbort, and F. Bullo, "Attention allocation for decision making queues," *Automatica*, vol. 50, no. 2, pp. 378–388, 2014.
- [20] M. Awad, R. Khanna, M. Awad, and R. Khanna, "Hidden Markov Model," *Efficient Learning Machines: Theories, Concepts, and Applications for Engineers and System Designers*, pp. 81–104, 2015.
- [21] Y. Bengio and P. Frasconi, "Input-output HMMs for sequence processing," *IEEE Transactions on Neural Networks*, vol. 7, no. 5, pp. 1231–1249, 1996.
- [22] D. H. Mangalindan, E. Rovira, and V. Srivastava, "On trust-aware assistance-seeking in human-supervised autonomy," in *2023 American Control Conference (ACC)*, pp. 3901–3906, 2023.
- [23] K. Akash, G. McMahon, T. Reid, and N. Jain, "Human trust-based feedback control: Dynamically varying automation transparency to optimize human-machine interactions," *IEEE Control Systems Magazine*, vol. 40, no. 6, pp. 98–116, 2020.
- [24] K. P. Murphy, "A survey of POMDP solution techniques," *Environment*, vol. 2, no. 10, 2000.
- [25] D. Braziunas, "POMDP solution methods," *University of Toronto*, 2003.
- [26] N. Koenig and A. Howard, "Design and use paradigms for Gazebo, an open-source multi-robot simulator," in *International Conference on Intelligent Robots and Systems*, vol. 3, pp. 2149–2154, IEEE, 2004.
- [27] M. Quigley, K. Conley, B. Gerkey, J. Faust, T. Foote, J. Leibs, R. Wheeler, and A. Y. Ng, "ROS: an open-source robot operating system," in *ICRA Workshop on Open Source Software*, vol. 3, p. 5, Kobe, Japan, 2009.
- [28] Y. Sakamoto, M. Ishiguro, and G. Kitagawa, "Akaike information criterion statistics," *Dordrecht, The Netherlands: D. Reidel*, vol. 81, no. 10.5555, p. 26853, 1986.
- [29] A. A. Neath and J. E. Cavanaugh, "The Bayesian information criterion: background, derivation, and applications," *Wiley Interdisciplinary Reviews: Computational Statistics*, vol. 4, no. 2, pp. 199–203, 2012.
- [30] M. M. M. Manhães, S. A. Scherer, M. Voss, L. R. Douat, and T. Rauschenbach, "UUV simulator: A Gazebo-based package for underwater intervention and multi-robot simulation," in *OCEANS Monterey*, pp. 1–8, 2016.